Metallurgical and Materials Engineering *Scientific paper*
Association of Metallurgical Engineers of Serbia AMES *https://doi.org/10.30544/327*

SYNTHESIS OF ASCORBIC ACID ENHANCED TIO_2 PHOTOCATALYST: ITS CHARACTERIZATION AND CATALYTIC ACTIVITY IN CO_2 PHOTOREDUCTION

M. F. Mohd Na'aim1, R. M. Ramli[1], N. A. Mohd Zabidi[2],*

[1]Chemical Engineering Department, Universiti Teknologi PETRONAS, 32610 Bandar Seri Iskandar, Perak, Malaysia
[2]Fundamental & Applied Science Department, Universiti Teknologi PETRONAS, 32610 Bandar Seri Iskandar, Perak, Malaysia

Received 16.10.2017
Accepted 23.03.2018

Abstract

To date, the development of solar environmental remediation has shifted more emphasis on the green and simple synthesis of catalyst for CO_2 photocatalysis process. Herein, TiO_2 photocatalyst was successfully synthesized via hydrothermal method. The effects of the different molar ratio of ascorbic acid $C_6H_8O_6$, (AA) added during the preparation of TiO_2 nanoparticles were comprehensively studied. The characterization of TiO_2 nanocrystals was performed via XRD, XPS, DRUV-vis, and FTIR. The results show the AA loading into TiO_2 nanoparticles significantly intensified the XRD spectra of anatase structure. In fact, this feature had signified a reactivity of the photocatalyst in the visible region. In an instance, BET surface area was also enhanced with the highest recorded value of 135.14 m^2/g for 0.8AA. Meanwhile, the CO_2 photoreduction over synthesized TiO_2 had produced the highest amount of HCOOH at 39.3 $\mu mol/g_{cat}$ for 0.8AA within 6 hours of reaction time. Furthermore, the DRUV-vis analysis had illustrated better light absorption ability of 0.8AA. This profound finding is attributed to the correlation between large surface area, pure anatase phase, and high adsorbed water molecules. Therefore, this study had significantly demonstrated the potential of modified TiO_2 with AA in CO_2 photocatalysis area while simultaneously presents a green and simple method for TiO_2 synthesis.

Keywords: CO_2 photoreduction; TiO_2; ascorbic acid; hydrothermal.

* Corresponding author: R. M. Ramli, *raihan.ramli@utp.edu.my*

Introduction

Recently, photocatalytic reduction of CO_2 provides a realistic insight to minimize atmospheric CO_2 while fulfilling the fuel production for world energy demand [1–4]. Virtually, TiO_2 photocatalyst has gained huge attraction for CO_2 photoreduction process owing to its reasonable price, non-toxic, chemically stable, and both optically and electronically stable [5].

Nevertheless, the low photon absorption of TiO_2 which is primarily in UV range only (2-5% of solar spectrum) had contributed to its inability to be efficient for visible region (43-45% of solar spectrum) [6]. Further, another primary concern is relatively poor adsorption of CO_2 on the surface of TiO_2 [7, 8]. In CO_2 photoreduction with H_2O, it is highly imperative to ensure the excited photogenerated electrons (e^-_{CB}) reduce adsorbed CO_2 into chemicals concerning their redox potentials and the positive holes (h^+_{VB}) oxidize water into O_2 and H^+ [3]. *Li et al.* [9] believed that specific distorted atom structure on the photocatalyst surface might positively influence the adsorption of CO_2 molecules onto the surface rather than H_2O molecules. Various ways have been explored to improve CO_2 adsorption capability onto the surface of TiO_2 such as facet engineering using Pt [1,4], hybrid adsorbent photocatalyst [7], graphene loaded TiO_2 [10] and acidified enhanced TiO_2 [11].

Despite the significant milestones achieved in synthesizing surface defect TiO_2, most of the previous studies require multi-step synthesis route including coupled hydrothermal-photodeposition [1], solvothermal followed by photodeposition and chemical reduction method [4], coprecipitation followed by hydrothermal treatment and modified Hummer's method followed by hydrothermal treatment [10]. Meanwhile, *He et al.* [11] synthesized TiO_2 simple hydrothermal method using hydrofluoric acid (HF) and further impregnated with sulfuric acid, H_2SO_4. Despite this, the usage of highly stable and toxic HF is dangerous, and a significant improvement is needed for the synthesis procedure of surface defect TiO_2.

Ascorbic acid, $C_6H_8O_6$ (AA) is one of the weak acid and widely used in various applications due to its mild nature and non-toxic properties [12, 13]. In this paper, a simple hydrothermal method is used to synthesize TiO_2 using titanium (III) chloride ($TiCl_3$) and ascorbic acid. Hence, the objective of this paper is to determine the effect of AA loading on the physiochemical properties TiO_2 catalysts and CO_2 photoreduction.

Experimental section

Chemicals and reagents

Chemicals used in this study are: titanium (III) chloride (15% $TiCl_3$ in 10% HCl, Merck), 99% L-ascorbic acid ($C_6H_8O_6$, R&M Chemicals); sodium hydroxide pellets (NaOH, Merck); calcium hydroxide [$Ca(OH)_2$, Acros Organic]; 95% denatured ethanol (C_2H_5OH, HmbG); sulfuric acid solution [$c(H_2SO_4)$ = 0.5 mol/L, Merck]; formic acid for analysis (HCOOH, Merck); and methanol for analysis (CH_3OH, Merck). The chemicals were used without further purification.

Synthesis Procedure

The synthesis of TiO_2 nanostructures was initiated by the addition of a different amount of ascorbic acid, $C_6H_8O_6$ (AA) to 100 mL of deionized water to achieve desired AA-TiO_2 molar ratio [14]. After 10 minutes of stirring, 7.20 g $TiCl_3$ was added to the solution. Then, 4 M NaOH solution was added until pH of the mixture increased to 4.0

[15]. Next, the mixture was treated with ultrasonication using an ultrasonic water bath (Bandelin, 300W, 35 kHz) at 35˚C for 1 hour [10]. The resulting suspension was then transferred equally into four Teflon-lined stainless-steel autoclave with a volume of 70mL and heated at 180 °C for 12 hours.

The autoclave was allowed to cool down to room temperature, and the precipitate was washed alternately three times with ethanol and water. The resultant slurry was dried in an oven (Memmert UF 110) for overnight at 80°C. The catalysts were denoted as *m*AA, where *m* was a molar ratio of $C_6H_8O_6$ to Ti. For example, TiO_2 with 0.493 g of $C_6H_8O_6$ with a molar ratio of 0.4 was represented by 0.4AA.

Nanoparticles characterization

The nanoparticles were characterized by powder X-ray Diffractometer (XRD), to determine the phases, present in the prepared TiO_2 powders. The diffraction patterns were analyzed using X'Pert3 Powder, PANalytical diffractometer with Cu Kα radiation at 45kV and diffracted beam monochromator at 40 mA, scanned from 10° to 90° in continuous mode at the intervals of 0.03° and with 0.3 s time steps. The crystallite sizes, D were calculated using Debye Scherrer's equation:

$$D = \frac{k\,\lambda}{\beta\cos\theta} \qquad 1$$

where k is a constant, assumed to be spherical, k = 0.9, λ is X-ray wavelength (λ= 1.5406 Å), β is full width at half maximum (FWHM) of major peak and θ is Bragg's diffraction angle [16].

A standard sample of $LaBr_6$ was used as a reference for diffractometer resolution function and line broadening to estimate the crystallite sizes [17]. Database ICDD PDF-2 was used to identify phases exist in the prepared TiO_2 [18]. Rietveld refinement was performed using HighScore Plus 4.2 software to determine the structural parameters of the synthesized TiO_2. The fitting considered the overall raw pattern compared to the conventional method of the experimental pattern. The analysis of surface functional groups was performed by Fourier Transform Infrared spectrometer (FTIR, Spectrum One, Perkin Elmer).

The N_2 adsorption-desorption isotherm was determined at 77 K using Surface Area and Pore Size analyzer (SAP, Micromeritics ASAP 2020). Before the measurement, the nanocrystal was degassed at 403 K for 4 hours. The elemental state of the synthesized catalyst was investigated using X-ray Photoelectron Spectrometer (XPS, Thermo Fisher K-Alpha) equipped with monochromatic Al Kα source (hυ = 1486.6 eV). The XPS spectra were analyzed using Thermo Scientific Avantage software. The peak fitting was performed using Gaussian–Lorentzian shapes with Shirley background subtraction [19].

The absorbance spectra were obtained using Diffuse Reflectance UV-visible spectroscopy (DRUV-vis, G9821A model, Agilent Cary 100) fitted with an integrated sphere. The absorbance analysis was conducted with a wavelength range of 200-800 nm under ambient condition and using $BaSO_4$ as a standard sample [20]. To estimate the band gap energies, the absorption edge of each respective catalyst was extrapolated to the x-axis of absorption wavelength (λ). The x-intercept was then substituted in the following equation [21]:

$$E_g = \frac{1239.8}{\lambda} \quad 2$$

where E_g is the band gap energy (eV), and λ is the edge wavelength (nm). The Kubelka-Munk function, F(R) against wavelength was also recorded using spectroscopy. Both graphs of $[F(R).h\upsilon]^{1/2}$ vs. hυ (indirect transition) and $[F(R).h\upsilon]^{2}$ vs. hυ (direct transition) were also plotted, and the estimated band gap values from both plots were compared to earlier band gap values (absorbance method).

CO_2 photoreduction with H_2O

Photocatalytic reduction of CO_2 was conducted in an ambient condition using halogen lamp (500 W, 1190 W/m^2) as visible light source and cooling fan was used to remove the heat from the lamp. The lamp was positioned 5 cm above a cylindrical glass reactor (height 10 cm, 5 cm diameter and total volume 100 cm^3) equipped with circular quartz window sealed with flange for absorption of light irradiation. The experiment was initiated by the addition of 0.105 g of TiO_2 catalyst into 70 mL of 0.1 mol/L $Ca(OH)_2$ solution (pH = 7.1 $\pm$ 0.1) in the reactor. Before the reaction, the pH value was adjusted with 0.005 mol/L H_2SO_4 solution.

Then, the catalyst was uniformly dispersed using a magnetic stirrer placed at the bottom of the reactor. Next, pure CO_2 gas (99.8% purity, Linde group) was bubbled into the solution at a flow rate of 200 mL/min for 30 minutes in the dark to saturate CO_2 in the medium and purge the reactor [6]. After 30 minutes, the reactor was sealed tightly, and the lamp switched on immediately to start the reaction. The photoreduction process was performed in batch mode during 6 hours reaction with CO_2 flow stopped at the beginning of the irradiation.

The reactor was placed in a water bath to control the temperature throughout the reaction, and soap bubble solution was used to check for any leakage exists in the experimental setup. 5mL of the products was collected by using a syringe at specific intervals and further filtered using 0.45 μm PTFE filter. The products were analyzed using High Precision Liquid Chromatography (HPLC, Agilent 1100). The equipment was fitted with both Refractive Index (RI, temperature = 35 °C) detector and UV detector (UV, 210nm).

For explicit quantification and accurate analysis, Transgenomic organic acid column (IC Sep ICE-ORH-801, 6.5 mm x 300 mm) was utilized in the product analysis with average column pressure and temperature of 94 bar and 65˚C respectively. The eluent used was 0.005 mol/L H_2SO_4 at a flow rate of 0.60 μL/min with a runtime of 20 minutes to detect all possible products that may exist. Both external standard (calibration curve) and internal standard (99% CH_3OH for analysis, 99% formic acid for analysis, Merck) were used to quantify the products.

Results and discussion

Fourier Transform Infrared (FTIR) analysis

Figure 1 shows the FTIR spectra of the prepared TiO_2 and P25 TiO_2. FTIR analysis examined the existence of functional groups in all photocatalysts.

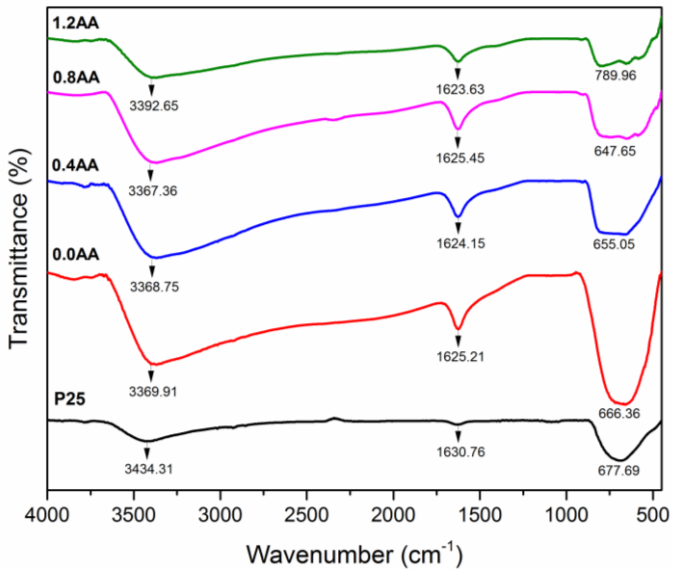

Fig. 1. FTIR spectra of P25 TiO_2 and synthesized TiO_2.

Figure 1 shows the consistent existence of TiO_2 spectrum in the low-frequency bands in the region of 500 cm^{-1} - 900 cm^{-1}. These broad absorption bands can be associated with the vibration of Ti–O–Ti bond which was supported by previous studies [21–23].

The sharp absorption bands of bending bond of water Ti-OH can be observed in the range of 1623.63 cm^{-1} to 1630.76 cm^{-1} with 0.4AA signified the lowest intensity among the synthesized catalysts [24,25]. Meanwhile, the stretching vibration of hydroxyl groups (O-H) with broad peaks between 3367.36 cm^{-1} and 3434.31 cm^{-1} can be attributed to adsorbed water molecules with the highest intensity of 0.8AA [26].

Besides, the intensity of surface –OH groups increased with increasing $C_6H_8O_6$ (AA) loading. This trend suggests that increasing AA loading had enhanced the adsorption of water molecules on the surface of TiO_2; this is in agreement with the recent study by *Tsai et al.* [23] which utilized HCl treatment in preparing TiO_2 nanostructures. In CO_2 photoreduction with H_2O, it is imperative to adsorb H_2O molecules onto TiO_2 surface due to induction of H^+ from the reaction between H_2O and holes [8]. The H^+ will be further reduced to •H radicals by photogenerated electrons, e^-_{CB} [3]. These •H radicals will further react with CO_2•$^-$ radicals to form possible products such as HCOOH, CH_3OH or HCHO.

X-ray diffraction (XRD) analysis

Figure 2 illustrates the XRD patterns of the P25 TiO_2 and TiO_2 nanoparticles. XRD analysis was performed to evaluate the effect of AA loading to the crystallinity of the synthesized TiO_2.

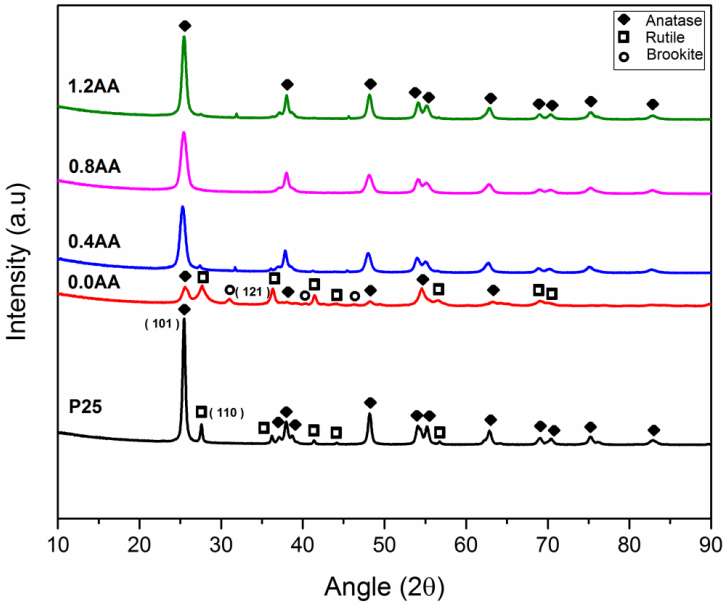

Fig. 2. XRD patterns of the TiO2 nanocrystals.

From Figure 2, it could be seen that all the synthesized TiO_2 and P25 TiO_2 have identical XRD patterns. Pure anatase phase was recognized in all enhanced TiO_2 (0.4AA, 0.8AA and 1.2AA).

Meanwhile, P25 TiO_2 was primarily formed in anatase phase with a small amount of rutile phase whereas, in 0.0AA, all three phases of rutile, brookite, and anatase were recorded in different proportions. The existence of brookite phase in bare TiO_2 without AA is by the result obtained by *Ren et al*. [14]. The prominent peak of (1 2 1) brookite was located at $2\theta = 30.9°$ (ICDD 01-080-7624).

Nevertheless, all catalysts have the main peak of (1 0 1) anatase at almost similar positions of 25.5°, 25.6°, 25.3°, 25.4°, and 25.4° of P25, 0.0AA, 0.4AA, 0.8AA and 1.2AA respectively (ICDD 01-089-4921, 01-075-2552, 01-076-3179, and 01-073-1764). Besides, the major peaks of (1 1 0) rutile appeared at 27.6° and 27.7° of P25 TiO_2 and 0.0AA respectively (ICDD 01-078-1510). The phase content, lattice parameters (a, b and c), full-width at half-maximum (FWHM total) and crystallite sizes based on major peaks of (1 0 1) anatase, (1 1 0) rutile and (1 2 1) brookite were summarized in Table 1.

Table 1. Structural parameters of TiO_2 nanocrystals.

Phase	Anatase					Rutile		Brookite
Structural parameters	P25	0.0AA	0.4AA	0.8AA	1.2AA	P25	0.0AA	0.0AA
Major peak	25.5˚	25.6˚	25.3˚	25.4˚	25.4˚	27.6˚	27.7 ˚	30.9˚
Major plane	(1 0 1)	(1 0 1)	(1 0 1)	(1 0 1)	(1 0 1)	(1 1 0)	(1 1 0)	(1 2 1)
Crsytallite size (nm)	23.4	9.8	11.3	10.6	14.9	35.5	9.8	14.6
Phase content (%)	89.0	17.6	100.0	100.0	100.0	11.0	61.2	21.2
FWHM total	0.3979	0.5314	0.7079	0.7698	0.5602	0.2440	0.9526	0.5218
a (Å)	3.7858	3.7761	3.7866	3.7863	3.7878	4.5937	4.6012	5.1451
b (Å)	a = b	a = b	a = b	a = b	a = b	a = b	a = b	9.1795
c (Å)	9.5074	9.4700	9.4935	9.4953	9.4985	2.9588	2.9549	5.4719

P25 TiO_2 was a binary mixture of 89.0% of anatase and 11.0% of rutile phase. Conversely, 0.0AA was a ternary mixture of 61.2%, 21.2%, and 17.6% of rutile, brookite, and anatase respectively. *Inada et al.* [27] discovered that the usage of autoclave could induce the formation of brookite crystals in the TiO_2 which was synthesized from the TiCl-based precursor. On the contrary, the addition of $C_6H_8O_6$ (AA) completely changed the phase of AA enhanced TiO_2 into pure anatase phase. *H-T Ren et al.* [14] highlighted that TiO_2 nanoparticle with a molar ratio of AA to Ti $\geq$ 0.25 were in pure anatase phase. In pure anatase phase, 0.8AA recorded the smallest crystallite size of 10.6 nm whereas the most significant crystallite size of 14.6 nm was recorded for 1.2AA in monophasic anatase system.

The addition of $C_6H_8O_6$ (AA) did affect the crystallographic structure of TiO_2 which was proven by a gradual increment of *c* value of lattice constant of anatase phase. Also, the FWHM total values also increased relatively with the standard P25 TiO_2. *Chen et al.* [28] asserted that the elevation in peak broadening could be due to the smaller size of TiO_2 nanocrystals compared with bulk TiO_2.

Brunauer-Emmett-Teller (BET) analysis

Table 2. BET/BJH analysis of TiO_2 nanocrystals.

TiO_2 nanocrsytals	S_{BET} (m^2/g)	Pore Volume (cm^3/g)	Pore size (nm)	Crystallite size anatase (nm)*	A/R/B composition (%)*
P25	49.02	0.2177	16.65	23.4	89.0/ 11.0
0.0AA	81.21	0.3648	14.66	9.8	17.6/ 61.2/ 21.2
0.4AA	107.12	0.2312	6.56	11.3	100.0
0.8AA	135.14	0.2594	5.76	10.6	100.0
1.2AA	93.52	0.2239	7.16	14.9	100.0

*From XRD data analysis

Table 2 presents the measured parameters from N_2 adsorption-desorption using ASAP Micromeritics 2020 equipment. It can be seen that addition of AA has significantly influenced the BET surface area, S_{BET} of the synthesized TiO_2. The highest recorded S_{BET} was 135.14 m^2/g of 0.8AA meanwhile the lowest S_{BET} was 49.02 m^2/g of

P25 TiO_2. Likewise, the measured S_{BET} value for P25 TiO_2 is similar to the reported value of 49.6 m^2/g as discovered by *Sosnov et al.* [29].

In fact, the S_{BET} values for all AA enhanced TiO_2 were significantly higher than P25 TiO_2. On the other hand, the S_{BET} value for 0.0AA was 81.21 m^2/g in which was lower compared to the S_{BET} values of modified TiO_2 nanocrystals – this could be caused by the content of brookite phase in 0.0AA as suggested by *Liu et al.* [30] previously. The mean pore size and pore volume were derived from Barrett-Joyner-Halenda (BJH) desorption, and pore size distribution is presented as depicted in Figure 3.

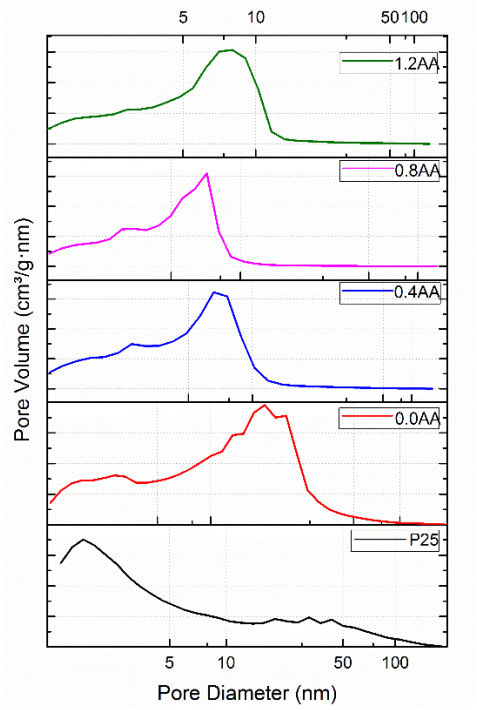

Fig. 3. BJH desorption dV/dD plot of all TiO2 nanocrystals.

Figure 3 indicated the mesoporous nature all TiO_2, where pore widths were in the range between 2 nm and 50 nm. Specifically, the range of pore diameter was between 5.76 nm and 16.65 nm and in accordance with IUPAC mesopores classification [31].

X-ray photoelectron spectrometer (XPS) analysis

XPS analysis was conducted to investigate the surface chemical states of the synthesized materials. XPS spectra revealing the classical peaks for Ti 2p are presented in Figure 4.

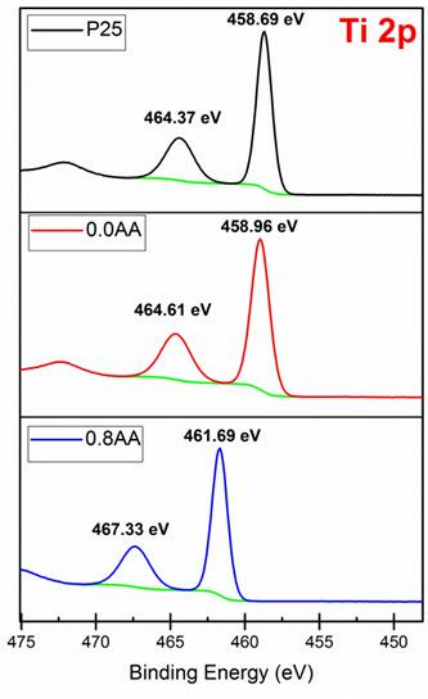

Fig. 4. XPS Spectra of Ti 2p of selected TiO_2 nanocrystals.

In Figure 4, the binding energy (BE) of Ti $2p_{3/2}$ and Ti $2p_{1/2}$ was indexed to 458.69 eV and 464.37 eV for P25 TiO_2. The values correspond to the presence of Ti(IV) oxide and close to the standard Ti $2p_{3/2}$ of 458.66 eV and Ti $2p_{1/2}$ of 464.31 eV [32]. A similar trend can trace for 0.0AA in which the peaks Ti $2p_{3/2}$ and Ti $2p_{1/2}$ were located at 458.96 eV and 464.61 eV respectively. Nevertheless, the addition of AA contributed to the peaks alteration of Ti^{4+} oxidation state, which was revealed by the peaks at 461.33 eV and 467.33 eV respectively. The BE shifted to a higher value in 0.8AA, and this implies that the TiO_2 lattice has been distorted by the interstitial doping of C in TiO_2 matrix. The result is in a good agreement with XRD analysis and recent research work by *S.K Warkhade et al.* [33].

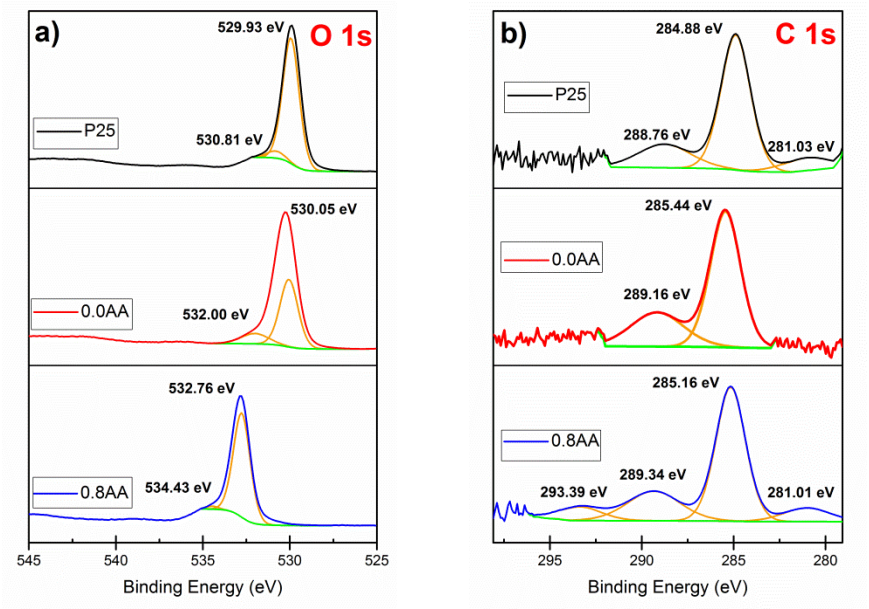

Fig. 2. XPS Spectra of selected TiO_2 nanocrystals: a) O 1s and b) C 1s.

Further explanation can be derived from XPS spectra of O 1s and C 1s as plotted in Figure 5(a) and 5(b). In Figure 5(a), typical peaks that reflect the lattice oxygen (Ti-O) presence were detected at 529.93 eV and 530.05 eV for P25 TiO_2 and 0.0AA respectively [34–36]. The peaks associated with oxygen bonded with metal (Ti-OH) or a surface hydroxyl group (-OH) were located at 530.81 eV and 532.00 eV for P25 TiO_2 and 0.0AA respectively [34–36]. Further evidence of interstitial incorporation of C in TiO_2 lattice was observed in 0.8AA at peaks of 532.76 eV and 534.43 eV. The recorded result is in agreement with FTIR spectra that show an increasing intensity of band ascribed with OH group. Moreover, *S. Warkhade et al.* [33] also concluded that TiO_2 distortion caused by C would elevate BE to a higher value.

Figure 5 (b) presents the deconvoluted XPS spectra of C 1s. Two mains peaks indexed to C-H bond or C-C bond and double bond C=O were 284.88 eV and 288.76 eV for P25 TiO_2 [36]. Identical peaks were also observed in 0.0AA at peaks of 285.44 eV and 289.16 eV [35]. Meanwhile, both peaks of 281.01 eV (0.8AA) and 281.01 (P25 TiO_2) were attributed to substitutional Ti-C bond as mentioned by *M.A. Mohamed et al.* [5]. New peak also emerged at 293.39 eV for 0.8AA which could be caused by the addition of AA.

Diffuse Reflectance UV-vis (DRUV-vis) analysis

DRUV-vis analysis was employed to investigate the light absorption properties of TiO_2 nanocrystals with standard reference of the P25 TiO_2 sample. Figure 6 displays the DRUV-vis plots of all TiO_2 nanocrystals which include the absorbance plot and Kubelka-Munk plots.

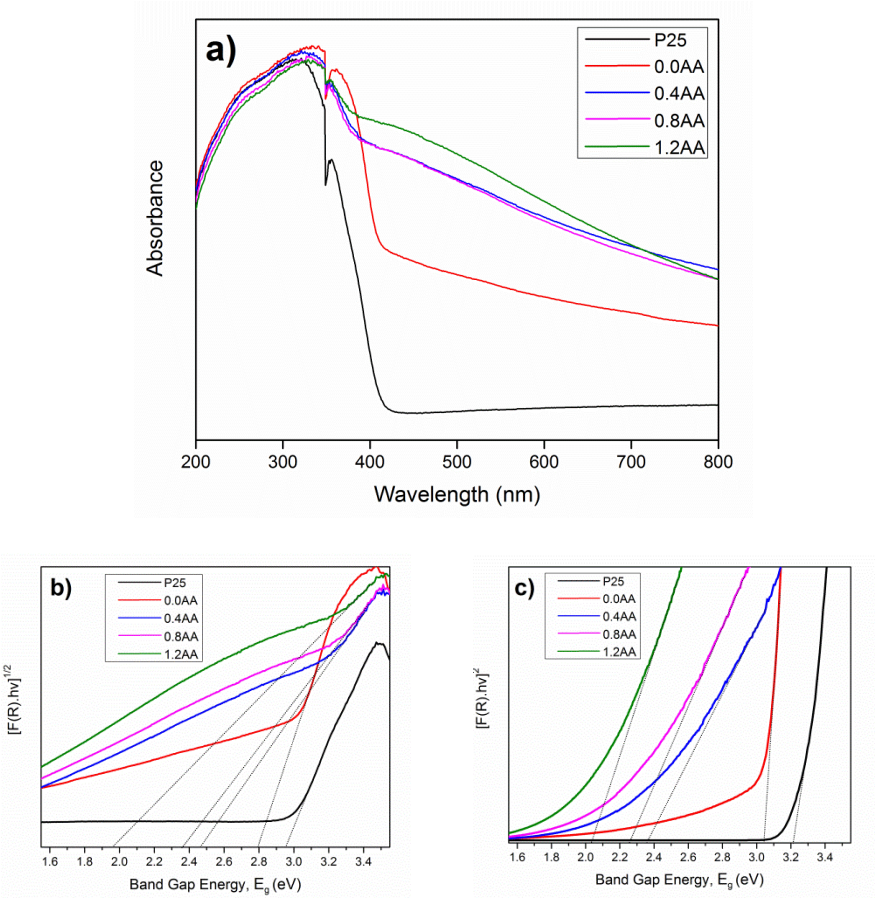

Fig. 3. DRUV-vis plot of all TiO_2 nanocrystals a) Abs vs. wavelength, b) Kubelka-Munk plot (indirect) c) Kubelka-Munk plot (direct).

To limit possible errors in the estimation of band gap energy (E_g), the values of Kubelka-Munk function F(R) were directly recorded from the DRUV-vis spectroscopy. Meanwhile, the usual practice is by converting the reflectance data (%R) into absorption mode as reported by several researchers [37–39]. Then, it will be plotted in Kubelka-Munk plot, $[(F(R).h\upsilon]^{1/n}$ vs $h\upsilon$ where n = 2 for indirect transition and n = ½ direct transition. In this case, the estimation of E_g has been conducted by from calculation from estimated absorption edge and both Kubelka-Munk plots as stated above.

In Figure 6(a), it is apparent that all TiO_2 samples including P25 have absorption edge beyond 400 nm. This finding contradicts to the previous research works which highlighted on absorption capability of P25 in UV region only (< 400 nm) [5,33]. In this case, the light absorption of all TiO_2 nanocrystals was shifted from 2.95 eV (P25 TiO_2) to 2.76 eV (0.0AA), 2.34 eV (0.4AA), 2.25 eV (0.8AA) and 2.00 eV (1.2AA). *M.A. Mohamed et al.* [5] previously stated that non-metal doping could induce a mid-gap

state which donates or receives electrons in the band gap of TiO_2. Hence, the addition of AA can distort TiO_2 lattice via C element and lower the band gap of TiO_2 [5,22,33].

Figure 6(b) and 6(c) show the Kubelka-Munk plot of indirect and direct transition respectively. It can be seen that the E_g values estimated from indirect transition were much lower compared to that of direct transition. Also, the calculated E_g values from indirect transition were much closer to the measured E_g values using absorbance method. The comparisons of E_g values from all three methods were summarized in Table 3, where the phase composition of crystalline phases was also provided.

Table 3. Estimated band gap energy (Eg) values for all TiO_2 nanocrystals with each respective phase composition.

TiO_2 nanocrsytals	E_g (eV) (absorbance)	E_g (eV) (indirect method)	E_g (eV) (direct method)	A/R/B composition (%)*
P25	2.95	2.96	3.21	89.0/ 11.0
0.0AA	2.76	2.79	3.04	17.6/ 61.2/ 21.2
0.4AA	2.34	2.47	2.36	100.0
0.8AA	2.25	2.36	2.26	100.0
1.2AA	2.00	1.96	2.04	100.0

*From XRD data analysis

To make the discussion more precise and straightforward, the E_g values measured from absorption edge have been utilized in this part. From Table 3, it can be suggested that the phase composition of TiO_2 significantly influences the E_g values, where all the AA-enhanced TiO_2 were in pure anatase phase and have E_g values less than 2.50 eV.

L. Cano-Casanova et al. [40] concluded that the higher the composition of anatase phase in TiO_2 nanocrystals, the lower the E_g values of respective TiO_2. In fact, *N. Sangiorgi et al.* [39] further strengthen the hypothesis by correlating the E_g values with lattice parameters, polycrystalline, amorphous phases and grain boundaries. Thus, the addition of AA to TiO_2 nanocrystals contributed to the alteration of TiO_2 crystallographic features and shifted the range of absorption into the visible region.

CO_2 photoreduction analysis

CO_2 photoreduction under visible light spectrum was conducted for 6 hours irradiation overall synthesized TiO_2 and P25 TiO_2 nanocrystals.

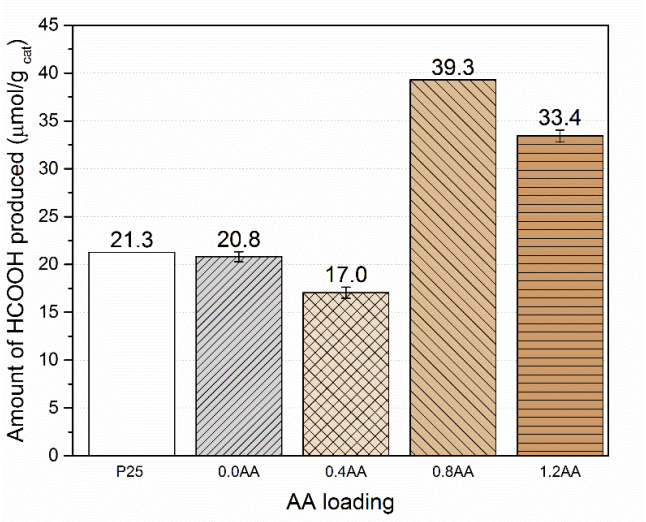

Fig. 4. Amount of HCOOH (normalized by catalyst mass) produced by CO_2 photoreduction with H_2O during 6 h visible light irradiation.

Control experiments were performed to validate the products obtained from the CO_2 photoreduction were only originated from CO_2. Firstly, the test only involved CO_2 and medium (limewater, $Ca(OH)_2$) in the dark and under light irradiation. No CO_2 possible reduction products were detected in both tests with or without light. Next, the P25 TiO_2 and all AA-enhanced TiO_2 were loaded into the reactor under light irradiation without any supply of CO_2. The same outcome was obtained as presented above. Identical control experiments were also conducted by recent research studies [4, 20, 38]. Thus, this indicates that bubbled CO_2 was the only carbon source in the reaction

On the contrary, only formic acid (HCOOH) was detected in the CO_2 photoreduction overall TiO_2 nanocrystals in 6 hours irradiation under visible light. Other possible products such as CH_3OH and HCHO were undetected. Figure 7 displays the amount of HCOOH produced from CO_2 photoreduction over TiO_2 nanocrystals. The best performing photocatalyst was 0.8AA with amount HCOOH produced of 39.3 μmol/$g_{cat.}$ The value almost doubled the amount of HCOOH produced by P25 which was 21.3 μmol/$g_{cat.}$ The sequence of HCOOH production by respective catalyst can be summarized as followed: 0.8AA>1.2AA>P25>0.0AA>0.4AA.

It was no coincidence that 0.8AA has the highest BET surface area, S_{BET} of 135.14 m^2/g compared to S_{BET} of 49.02 m^2/g of P25. However, the BET surface area is not the only determining factor of CO_2 photoreduction since 0.4AA has the lowest HCOOH production of 17.0 μmol/g_{cat} despite possessing high BET surface area (S_{BET} = 107.12 m^2/g). Moreover, 0.4AA has the lowest intensity of Ti-OH bending bond in FTIR analysis compared to the other synthesized TiO_2. *J. Low et al.* [41] asserted that one of the critical aspects in CO_2 photoreduction is the adsorption ability of TiO_2 towards CO_2 molecules. Thus, lack of Ti-OH bond can significantly affect the CO_2 photoreduction process.

Nevertheless, the crystalline composition also contributes to the effectiveness of CO_2 photoreduction with H_2O. *Liu and Li* [42] summarized that efficient charge transfer and separation between anatase and rutile strongly enhances CO_2 photoreduction over a binary mixture of anatase-rutile (P25) compared to monophasic anatase or rutile. Another essential point is the light absorption ability of TiO_2 in the visible region. Both 0.8AA and 1.2AA have much lower E_g values of 2.25 eV and 2.00 eV, which enable them to absorb light from the visible region and contribute to more significant HCOOH production. The results proved that CO_2 photoreduction is an integrated reaction which involves several determining factors CO_2 such as surface area, crystalline composition, crystallite size and also light harvesting properties [7, 43].

Conclusions

In conclusion, visible light responsive TiO_2 has been successfully fabricated in simple hydrothermal procedure with the incorporation of ascorbic acid, $C_6H_8O_6$ (AA). The characterization results had signified the TiO_2 lattice distortion by the incorporation of C element. Besides, the BET surface area, S_{BET} was also proportionally increased with the increment of AA loading with the highest S_{BET} value of 135.14 m^2/g for 0.8AA. Notably, the addition of AA has significantly affected the light harvesting ability and induced a red shift in the absorption edge of the TiO_2 nanocrystals. In fact, the highest amount of HCOOH produced over 6 hours visible light irradiation was 39.3 $\mu mol/g_{cat}$ for 0.8AA. Moreover, the obtained HCOOH amount was almost 50% higher compared to the obtained HCOOH amount of P25 TiO_2. However, further investigation should be conducted to find the right combination of anatase crystallite size, visible light harvesting, surface area, and nature of the catalyst and optimal pH of the reaction medium.

Acknowledgments

The authors would like to express their gratitude to Universiti Teknologi PETRONAS (UTP) for the financial support provided through Short Term Internal Research Fund (STIRF) (0153AA-D56). Special thanks to Centralized Analytical Laboratory (CAL), for the characterization analysis.

References

[1] J. Mao, L. Ye, K. Li, X. Zhang, J. Liu, T. Peng, L. Zan: Appl Catal B Environ, 144 (2014) 855–862.
[2] E. Karamian, S. Sharifnia: J CO_2 Util, 16 (2016) 194–203.
[3] H. Abdullah, M. M. R. Khan, H. R. Ong, Z. Yaakob: J CO_2 Util, 22 (2017) 15–32.
[4] Z. Xiong, Z. Lei, X. Chen, B. Gong, Y. Zhao, J. Zhang, C. Zheng, J. C. S. Wu: Catal Commun, 96 (2017) 1–5.
[5] M. A. Mohamed, W. N. Wan Salleh, J. Jaafar, M. S. Rosmi, Z. A. Mohd. Hir, M. Abd Mutalib, A. F. Ismail, M. Tanemura: Appl Surf Sci, 393 (2017) 46–59.
[6] D. O. Adekoya, M. Tahir, N. A. S. Amin: J CO_2 Util, 18 (2017) 261–274.
[7] H. Zhao, J. Xu, L. Liu, G. Rao, C. Zhao, Y. Li: J CO_2 Util, 15 (2016) 15–23.
[8] H. Zhao, F. Pan, Y. Li: J Materiomics, 3 (2017) 17–32.
[9] K. Li, X. An, K. H. Park, M. Khraisheh, J. Tang: Catal Today, 224 (2014) 3–12.
[10] Q. Zhang, C. F. Lin, B. Y. Chen, T. Ouyang, C. T. Chang: Environ Sci Technol, 49 (2015) 2405–2417.

[11] Z. He, J. Tang, J. Shen, J. Chen, S. Song: Appl Surf Sci, 364 (2016) 416–427.
[12] J. Zhang, H. Yang, G. Shen, P. Cheng, J. Zhang, S. Guo: Chem Commun, 46 (2010) 1112–1114.
[13] X. Zhu, Q. Liu, X. Zhu, C. Li, M. Xu, Y. Liang: Int J Electrochem Sci, 7 (2012) 5172–5184.
[14] H. T. Ren, S. Y. Jia, S. H. Wu, Y. Liu, X. Han: Mater Lett, 101 (2013) 69–71.
[15] M. Wajid Shah, Y. Zhu, X. Fan, J. Zhao, Y. Li, S. Asim, C. Wang: Sci Rep, 5 (2015) 1–8.
[16] S. Tada, F. Watanabe, K. Kiyota, N. Shimoda, R. Hayashi, M. Takahashi, A. Nariyuki, A. Igarashi, S. Satokawa: J Catal, 351 (2017) 107–118.
[17] V. Likodimos, A. Chrysi, M. Calamiotou, C. Fernández-Rodríguez, J. M. Dona-Rodríguez, D. D. Dionysiou, P. Falaras: Appl Catal B Environ, 192 (2016) 242–252.
[18] M. Dimitrov, R. Ivanova, N. Velinov, J. Henych, M. Slušná, V. Štengl, I. Mitov: Nano-Structures & Nano-Objects, 7 (2016) 53–63.
[19] A. A. Ismail, R. A. Geioushy, H. Bouzid, S. A. Al-Sayari, A. Al-Hajry, D. W. Bahnemann: Appl Catal B Environ, 129 (2013) 62–70.
[20] L.-L. Tan, W.-J. Ong, S.-P. Chai, B. T. Goh, A. R. Mohamed: Appl Catal B Environ, 179 (2015) 160–170.
[21] Z. Li, X. Cao, C. Ma, R. Gao, T. Sun, C. Li: Mater Lett, 184 (2016) 123–126.
[22] H. M. Yadav, J. Kim: J Alloys Compd, 688 (2016) 123–129.
[23] C. Y. Tsai, C. W. Liu, Y. H. Chan, T. Y. Chang, B. C. Chen, H. C. His: Catal Today, 297 (2017) 113–123.
[24] R. Fagan, D. W. Synnott, D. E. McCormack, S. C. Pillai: Appl Surf Sci, 371 (2016) 447–452.
[25] A. León, P. Reuquen, C. Garín, R. Segura, P. Vargas, P. Zapata, P. Orihuela: Appl Sci, 7 (2017) 1–9.
[26] M. Bagher, Z. Tavakoli, M. Seifi, M. B. Askari, Z. Tavakoli Banizi, M. Seifi, S. Bagheri Dehaghi, P. Veisi: Optik (Stuttg), 149 (2017) 447–454.
[27] [M. Inada, K. Iwamoto, N. Enomoto, J. Hojo: J Ceram Soc Japan, 119 (2011) 451–455.
[28] K. Chen, Z. Jiang, J. Qin, Y. Jiang, R. Li, H. Tang, X. Yang: Ceram Int, 40 (2014) 16817–16823.
[29] E. a. Sosnov, K. L. Vasil'eva, A. A. Malkov: Russ J Phys Chem A, 84 (2010) 1028–1032.
[30] L. Liu, D. T. Pitts, H. Zhao, C. Zhao, Y. Li: Appl Catal A Gen, 467 (2013) 474–482.
[31] M. Thommes, K. Kaneko, A. V Neimark, J. P. Olivier, F. Rodriguez-reinoso, J. Rouquerol, K. S. W. Sing: IUPAC Technical Report (2015).
[32] M. C. Biesinger, L. W. M. Lau, A. R. Gerson, R. S. C. Smart: Appl Surf Sci, 257 (2010) 887–898.
[33] S. K. Warkhade, G. S. Gaikwad, S. P. Zodape, U. Pratap, A. V Maldhure: Mater Sci Semicond Process, 63 (2017) 18–24.
[34] M. Park, B. S. Kwak, S. W. Jo, M. Kang: Energy Convers Manag, 103 (2015) 431–438.
[35] M. Tahir, B. Tahir: Appl Surf Sci, 377 (2016) 244–252.
[36] M. Tahir, B. Tahir, N. A. S. Amin, Z. Y. Zakaria: J CO_2 Util, 18 (2017) 250–260.
[37] A. Dolgonos, T. O. Mason, K. R. Poeppelmeier: J Solid State Chem, 240 (2016) 43–48.

[38] K. A. Ali, A. Z. Abdullah, A. R. Mohamed: Appl Catal A Gen, 537 (2017) 111–120.
[39] N. Sangiorgi, L. Aversa, R. Tatti, R. Verucchi, A. Sanson: Opt Mater (Amst), 64 (2017) 18–25.
[40] L. Cano-Casanova, A. Amorós-Pérez, M. Ouzzine, M. A. Lillo-Ródenas, M. C. Román-Martínez: Appl Catal B Environ, 220 (2018) 645–653.
[41] J. Low, B. Cheng, J. Yu: Appl Surf Sci, 392 (2017) 658–686.
[42] L. Liu, Y. Li: Aerosol Air Qual Res, 14 (2014) 453–469.
[43] Y. Sohn, W. Huang, F. Taghipour: Appl Surf Sci, 396 (2017) 1696–1711.